Catalyst screening for the Oxidative Coupling of Methane: from isothermal to adiabatic operation via microkinetic simulations

Laura Pirro[†], *Pedro S. F. Mendes*[†], *Bart D. Vandegehuchte*[‡], *Guy B. Marin*[†], *Joris W. Thybaut*[*,†]

† Laboratory for Chemical Technology, Ghent University, Technologiepark 125, B-9052 Ghent, Belgium

‡ Total Research & Technology Feluy, Zone Industrielle Feluy C, B-7181, Seneffe, Belgium

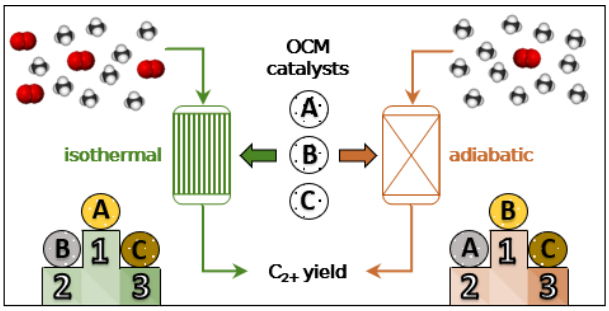

OCM catalysts underperforming in typical isothermal conditions could result in above average performances in adiabatically-relevant operating conditions

Abstract

A microkinetics-based study was performed on the relevance of conventional isothermal data for the selection of catalysts for Oxidative Coupling of Methane (OCM) in adiabatic reactors. Catalyst performances from isothermal tests in oxygen-lean feeds ($CH_4/O_2 \geq 7$) were found to reliably indicate the catalyst ranking for adiabatic operation, which features large methane excess for temperature control reasons. In oxygen-lean operation, a lower contribution of surface reactions is beneficial for the selectivity at iso-conversion. Hence, the concentration of surface oxygen was found to be significantly lower on the top-performing catalysts at higher methane-to-oxygen ratios. However, these relevant isothermal data are scarce in literature because typically oxygen-rich ($CH_4/O_2< 5$) reaction conditions are used to maximize the C_{2+} yield. Therefore the majority of lab-scale tests at isothermal conditions might have resulted in the rejection of catalysts that could perform reasonably well at conditions typical for adiabatic reactors. The insights gained via kinetic and statistical analysis were further elaborated to suggest experimental guidelines for future isothermal benchmarking of OCM catalysts in view of the industrially-relevant adiabatic operation.

1. Introduction

In the past decade, shale gas has assumed a predominant role in the world economy[1] and its impact on the energy and chemical markets is forecasted to increase even more in the next years[2]. Major efforts are currently focused on processes for direct conversion of methane, which are regarded as promising but challenging alternatives to the syngas route to chemicals[3]. Among those direct conversion processes, the Oxidative Coupling of Methane (OCM)[4] is appealing for direct ethylene production, a key building block in the chemical industry[5]. However, since its conception[6], the industrial development of OCM has been hampered by the trade-off between methane conversion and C_2 selectivity[7]. The oxidation of methyl radicals to carbon oxides

(primary oxidation) competes with radical coupling to ethane. In addition, the oxidation of ethane and ethylene takes place extensively as these products are more reactive than methane itself (consecutive oxidation)[8]. This issue represents a recurring theme in methane activation and functionalization research, which goes well beyond OCM[9], and for which optimal solutions are still to be found. The need to address these challenges has driven many of the studies on catalyst[10] and reactor[11] optimization. An abundance of catalytic data has been collected up to now mainly in laboratory-scale fixed-bed reactors. Isothermal mode was targeted in most cases not to complicate the observations by the pronounced exothermicity of the reaction[12], and to extract mechanistic and kinetic information deprived of thermal effects[13]. A database recently reported by Schmack et al.[14] is visualized in Figure 1, wherein C_2 selectivity is represented as a function of CH_4 conversion for a broad variety of catalytic materials in a wide range of operating conditions.

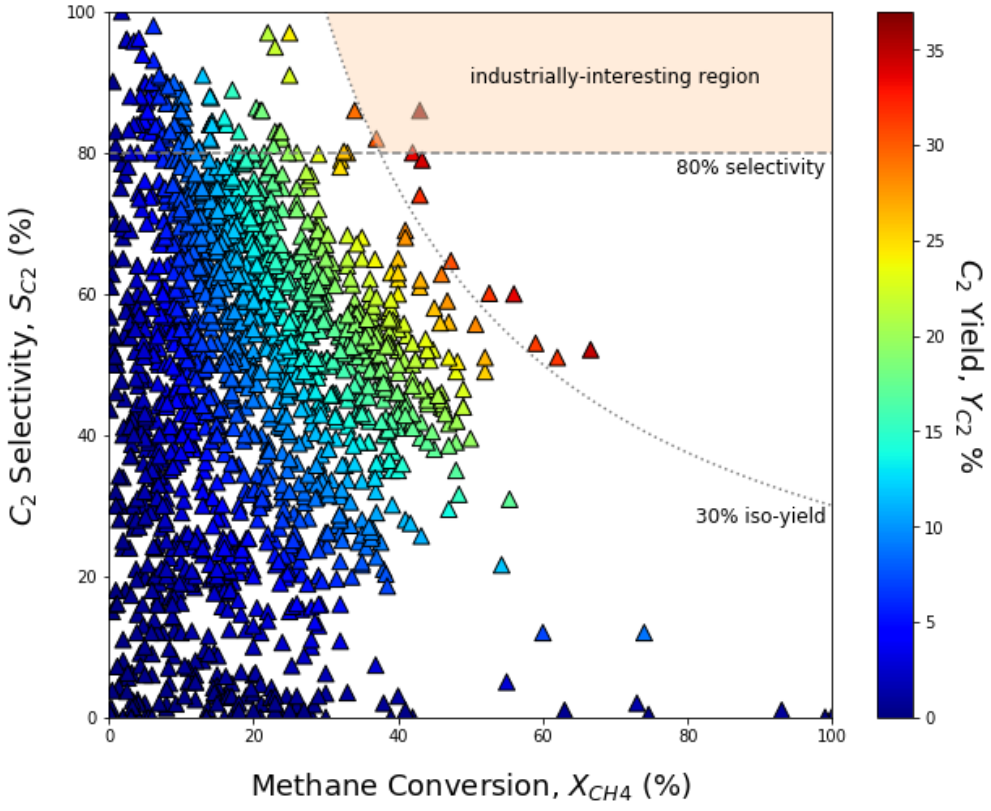

Figure 1. Overview of the experimental data obtained for OCM in laboratory-scale isothermal fixed-bed reactors, in terms of C_2 selectivity as function of CH_4 conversion (operating conditions: T= 773 – 1223 K, CH_4/O_2= 0.9 – 38.3, GHSV= 350000 – 20 h^{-1}, p= 1 – 4.5 bar). This figure includes 1802 datapoints, based on the data provided by Schmack et al.[14].

It is striking that almost all datapoints are located outside of what is considered to be the industrially-feasible target of >30% C_2 yield at a C_2 selectivity of >80%[15]. This is a clear indication that for OCM, as well as for other methane direct valorisation processes[16], catalyst design needs to be complemented by developments on the reactor and process level to advance on the selectivity-conversion trade-off.

The Siluria OCM process[17], very recently acquired by McDermott[18], contains an adiabatically operated fixed-bed reactor at the heart of the proposed process configuration[19]. This seems to point to adiabatic fixed-bed reactors, rather than isothermal multi-tubular ones, as a viable option for large-scale OCM implementation[20]. While a few related studies have been carried out decades ago[21-23], adiabatic OCM reactors have recently received increasing academic and industrial attention[24-33]. The main driver is the exploitation of the reaction exothermicity to lower the inlet temperature required and, ideally, operate the reactor autothermally.

As the majority of catalytic studies focused on isothermal operation, considerable research efforts are now required to design adequate catalysts for adiabatic operation. Aiming at building up on the isothermal studies, a very relevant question is whether catalysts that have exhibited the best performances in isothermal conditions would also serve as best candidates in an adiabatic reactor. In other words: given a certain ranking of catalytic materials according to a specific performance parameter, would this ranking be preserved when moving from isothermal to adiabatic operation?

The main goal of the present work is, hence, the identification of isothermal bench scale data that are most informative for extrapolation towards adiabatic industrial operation. This was pursued by evaluating the impact of operating conditions on the catalyst performance ranking using microkinetic simulations, for both isothermal and adiabatic operation. Microkinetic models are reputed as excellent tools for the simultaneous screening of catalyst properties and operating conditions[34], given a specific reactor configuration[35]. A major advantage of such a

modelling approach is the possibility of comparing performance data in truly isothermal and truly adiabatic conditions. As described elsewhere[36, 37], perfect isothermicity, which is often claimed in publications, is actually very hard to realize in OCM fixed-bed setups. On the other hand, due to heat losses[33], perfect adiabatic operation is difficult to achieve in bench-scale setups, while heat losses become negligible on the industrial-scale[24]. Simulated performance data can level out non-idealities in reactor operation and enable a direct comparison of intrinsic performances of different catalysts. This clear-cut approach allows catalyst benchmarking on a theoretical base.

In the first section of the present work, an overview of the methodological workflow for OCM catalysts ranking based on microkinetic simulations is provided. Subsequently, the impact of operating conditions on the catalyst ranking is analysed: first, for a broad range of isothermal cases; next for a more limited number of selected adiabatic cases; and finally by comparing results for both operating modes. In the discussion section, a broader perspective on isothermal experimental data from literature is presented, and guidelines for catalyst screening targeting adiabatic fixed-bed operation are provided.

2. Methodology for OCM catalysts ranking via microkinetic simulations

2.1 Overall workflow

The workflow adopted for ranking OCM catalysts is depicted in Figure 2, both for isothermal and adiabatic operation. The workflow is composed of three main steps: 1. microkinetic simulations for a high number (> 200) of OCM catalysts; 2. ranking of the catalysts by normalization of the obtained C_{2+} yields; 3. pairwise comparisons via statistical analysis.

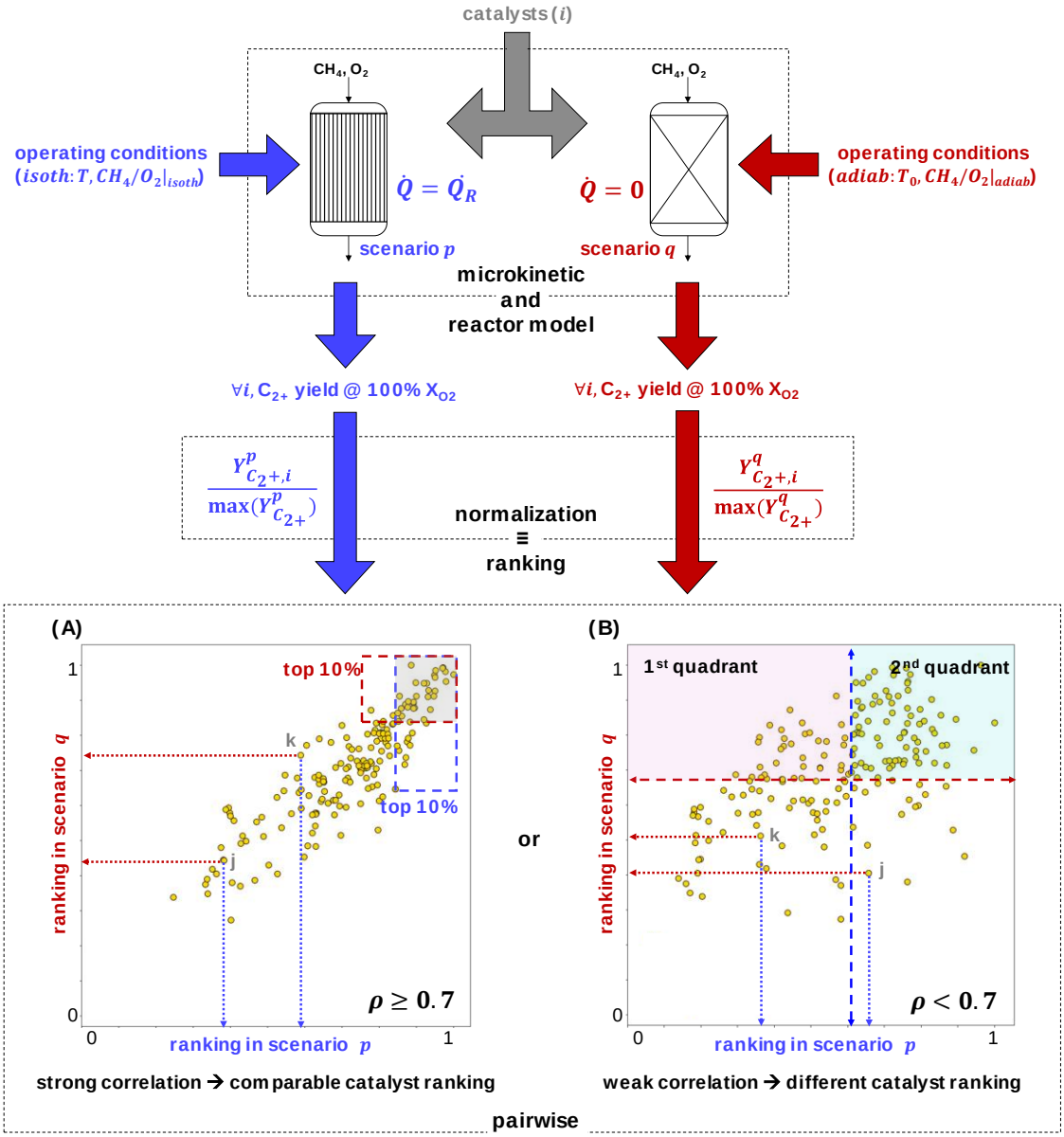

Figure 2. Methodology adopted for catalysts ranking and pairwise comparison of operating modes. C_{2+}: C_2H_6, C_2H_4, C_2H_2, C_3H_8, C_3H_6, $\dot{Q}$: thermal power exchanged with the surroundings, $\dot{Q}_R$: thermal power generated by the reaction, X_{O2}: oxygen conversion, Y: yield, ρ: Pearson's correlation coefficient. (The analysis of the top 10% catalysts was performed in every case, but it is herein indicated only for the strong correlation case (A) for the sake of visual simplicity.)

Microkinetic simulations

A microkinetic model for the OCM reaction, previously developed by our group[38], is embedded in a fixed-bed reactor model which allows the simulation of both isothermal and adiabatic operation[28]. this Both the kinetic and the reactor model were extensively described in the referenced literature and an overview is provided in section S1 of the S.I.. The microkinetic model was validated for several OCM catalysts[39], by varying sixteen parameters denoted as

catalyst descriptors[40]. These descriptors, obtained via regression towards experimental data, are defined as properties which directly impact the reaction kinetics and depend on the catalyst[41]. These include, among others, chemisorption enthalpies, sticking coefficients, density of active sites. This definition is different from others adopted in literature, which might refer to transition state energetic parameters from theoretical calculations, such as the C-H bond dissociation energy and the oxygen vacancy formation energy[42], physico-chemical catalyst properties, such as the ability to form a carbonate and the thermal stability of this carbonate[14], or, as in machine learning works, descriptor can have an even more general meaning, such as preparation method and operating conditions[43].

In this work, the performance of real catalysts could be reproduced via realistic combinations of catalyst descriptors (see also section 2.2), in the hypothesis of stable operation of the catalysts in all the investigated operating conditions. As input for the microkinetic and reactor model, the descriptors of each catalyst i and the operating scenarios are required. The operating scenarios, indicated by p and q, are defined as the reactor operating mode (isothermal or adiabatic) and the set of operating conditions considered. In Figure 2, an isothermal scenario p, with operating conditions $isoth=(T, CH_4/O_2|_{isoth})$, and an adiabatic scenario q, with operating conditions $adiab=(T_0, CH_4/O_2|_{adiab})$, are considered, see also section 2.2 for the selection of the operating conditions. It should be mentioned that all the simulated scenarios refer to co-feed operation, where both CH_4 and O_2 are simultaneously fed to the reactor. This means that molecular oxygen from the gas phase is required for methane activation and that the catalysts do not undergo any cyclic operation in reduction−oxidation reactor modes[44]. The model output is a set of key performance indicators for catalyst i and scenario j. The yield of C_{2+} products (C_2H_6, C_2H_4, C_2H_2, C_3H_8, C_3H_6) at the reactor outlet, $Y^{j}_{C_{2+},i}$, is the focus of the present work.

Catalysts ranking

The ranking of catalyst i in scenarios p and q is defined as the normalized C_{2+} yield, $\frac{Y^p_{C_{2+},i}}{\max(Y^p_{C_{2+}})}$ and $\frac{Y^q_{C_{2+},i}}{\max(Y^q_{C_{2+}})}$, respectively. The ranking can assume values in the interval [0,1], with the best performing catalyst in each scenario attaining a ranking of 1 and catalysts, if any, with zero yield attaining ranking 0.

Pairwise comparisons of operating scenarios

The comparison of these rankings is carried out using the Pearson's correlation coefficient ρ[45], which measures the linear correlation between two variables:

$$\rho = \frac{\sum_{i=1}^{n}(P_i - \bar{Q})(Q_i - \bar{P})}{\sqrt{\sum_{i=1}^{n}(P_i - \bar{P})^2}\sqrt{\sum_{i=1}^{n}(Q_i - \bar{Q})^2}}$$

$P_i = \frac{Y^p_{C_{2+},i}}{\max(Y^p_{C_{2+}})}$: ranking of catalyst i in scenario p

$Q_i = \frac{Y^q_{C_{2+},i}}{\max(Y^q_{C_{2+}})}$: ranking of catalyst i in scenario q

n: number of catalysts (= 220)

$\bar{P} = \frac{1}{n}(\sum_{i=1}^{n} P_i)$: mean ranking in scenario p

$\bar{Q} = \frac{1}{n}(\sum_{i=1}^{n} Q_i)$: mean ranking in scenario q

This comparison is visualized in a pairwise ranking graph, in which the catalyst ranking in scenario q (y-axis) is plotted against the catalyst ranking in scenario p (x-axis). Each point in the graph represents one of the n catalysts. These points are shown in yellow in case of comparison between an isothermal and an adiabatic scenario (such as in Figure 2 and in section 3.2), in green in case of two isothermal scenarios being compared (section 3.1), and in orange for two adiabatic scenarios (section S5 in S.I.).

According to literature guidelines[46], a typical value $\rho = 0.7$ was chosen as a threshold of strong positive correlation. However, rather than the exact value, the qualitative trends in ρ as a function of the operating conditions were considered of main interest. A strong correlation, such as in Figure 2 – case A, indicates that the catalyst ranking is not affected by a particular change in operating mode or conditions.

As indicated in Figure 2 – case A, particular attention was paid to the top 10% performing catalysts in each scenario, indicated by the dashed boxes. The impact of the operating conditions on the top 10% catalysts ranking is represented by the extent of the overlap between the two boxes (shaded area in the figure). The visual interpretation was supported by statistical testing[47, 48], to identify descriptors that discriminate between both catalyst groups of interest, as described in detail in previous work[49]. In case of weak correlation between the performances in the investigated scenarios, such as in Figure 2 – case B, an additional analysis was performed, to gain further insights into the cause of the spread in the data. Based on the median performance obtained in each scenario (indicated by dashed arrows in the figure), the descriptors of catalysts with ranking above the median value in only one of the two scenarios (in practice, the 1st quadrant catalysts) were compared to the catalysts characterized by above-median ranking in both scenarios (2nd quadrant catalysts).

2.2 Catalysts and operating conditions

The performances of several OCM catalysts reported in literature were reproduced in the microkinetic simulations herein via a methodology previously developed in our research group, encompassing both microkinetics and statistical testing[49]. A total of 220 realistic catalyst descriptors combinations, corresponding to a variety of real OCM catalysts, were identified starting from six literature datasets: two datasets from the work of Kondratenko et al.[50], two datasets from the work of Olivier et al.[51], one dataset from the work of Huang et al.[52] and one dataset from the work of Shahri and Pour[53]. These datasets were selected because of the broad

variety of catalytic materials which were experimentally tested, see Table S2.1 of the S.I.. Additional details about the real catalysts from the literature datasets and the methodology adopted to identify the realistic catalyst descriptor combinations are reported in section S2 of the S.I..

Concerning the operating conditions adopted for the simulations, a summary is reported in Table 1. The selection of operating conditions for isothermal operation was based on available literature data. Out of the 1802 experiments reported by Schmack et al.[14], more than 61% of the data (1115 datapoints) was obtained in the operating range: CH_4/O_2= 2-10, T= 1023-1173 K (at atmospheric pressure, with gas hour space velocity ranging from 350 to 350000 h^{-1} and nitrogen dilution in the range of 0% - 95%). These temperature and feed composition ranges sufficiently cover the majority of conditions applied in literature for OCM experiments. It is worth mentioning that less than 10% of the literature data was obtained at CH_4/O_2 molar ratios exceeding 5 and temperatures higher than 1073K, while approx. 33% of the data points fall in the range: CH_4/O_2= 2-5, T= 1023-1073 K. The latter can, hence, be considered as the 'typical' operating range in isothermal OCM literature.

Table 1. Operating conditions considered for the microkinetic simulations.

operating scenario	**p [bar]**	**GHSV [10^3 h^{-1}]**	**T (isoth)/T_0 (adiab) [K]**	**CH_4/O_2 [mol/mol]**	**Ref.**
isothermal	1.013	1 -300	1023, 1073, 1123, 1173	2,3,4,5,6,7,8,9,10	[14]
adiabatic			800, 853, 900	9, 9.8, 11	[28]

The selection of the operating conditions for the adiabatic scenarios has been discussed in detail in our previous work[28]. The maximum temperature in the reactor was set to 1273 K based on metallurgical constraints for stainless steel[54]. Furthermore, it is considered unlikely that OCM catalysts are stable at temperatures exceeding this value[55]. By fixing the maximum temperature, the number of degrees of freedom was reduced by one, as only one combination of inlet temperature T_0 and feed composition would allow a maximum temperature of 1273 K at the

reactor outlet. The adiabatic temperature rise ΔT_{ad}, related to the reaction exothermicity, allows values of T_0 which are usually too low for isothermal OCM (i.e. < 923 K). Three sets of adiabatic conditions were, hence, considered: T_0= 800 K and CH_4/O_2= 9.0, T_0= 853 K and CH_4/O_2= 9.8, T_0= 900 K and CH_4/O_2= 11.0. Similarly as in previous work[28], atmospheric pressure was considered, in view of C_{2+} selectivity maximization[56], both for the isothermal and the adiabatic scenarios.

Oxygen being the limiting reactant, the catalyst ranking was performed at comparable oxygen conversion and the GHSV was adapted correspondingly for each catalyst. More precisely, full oxygen conversion is a pre-requisite of a relevant OCM process, to ensure safe operation of the downstream sections of the plant[57]. Hence, for each set of conditions, the maximum GHSV ensuring complete oxygen conversion at the reactor outlet was used. As in previous work, a minimum GHSV of 1000 h^{-1} was considered in view of economic viability[58]. Specifically for adiabatic operation, in case a GHSV of 1000 h^{-1} was found to be insufficient to reach the full oxygen conversion, due to the low inlet temperatures considered, this aspect was explicitly taken into account in subsequent data interpretation.

3. Results

The impact of operating conditions on the catalyst ranking for isothermal and adiabatic scenarios are presented individually in section 3.1 and compared in section 3.2.

3.1 Impact of operating conditions on the catalyst ranking

A stepwise approach was taken in the analysis of the isothermal rankings: catalyst performances were first simulated within a narrow range of operating conditions, which was progressively expanded to evaluate differences in catalysts ranking, if any.

Typical conditions were selected for two isothermal scenarios, i.e. lower temperatures and low methane-to-oxygen ratios. Simulation results for both scenarios are reported in Figure 3/A. A

very strong correlation ($\rho = 0.96$) can be observed, thus indicating that the catalyst ranking is not significantly affected by the change in the operating conditions. This is also evident from the top 10% performing catalysts, which are essentially the same in the two scenarios. A similar conclusion can be drawn from a more extended analysis of various isothermal scenarios in the typical operating range (T= 1023-1073 K, CH_4/O_2= 2-5), as reported in section S3 of the S.I. This suggests that catalyst selection for the most commonly adopted set of isothermal operating conditions is valid for other conditions within the above range.

The interest in adiabatic operation implies the need to evaluate also isothermal results in a broader temperature range and at oxygen-lean feed compositions. Pairwise comparisons of isothermal scenarios within the ranges T= 1023-1173 K and CH_4/O_2= 2-10 can result in less pronounced correlations ($\rho = 0.65$) as evident from the large spread in data, illustrated in Figure 3/B for the extreme conditions. In these extreme scenarios, the catalyst ranking is significantly impacted by the difference in operating conditions, which is also evidenced by the top 10% catalysts exhibiting significant differences. Similar observations were found when comparing slightly different operating scenarios (Figure S3.1/B).

Due to the variation in both operating conditions, i.e., operating temperature and methane-to-oxygen ratio, the origin of the discrepancy in catalyst ranking between these two extreme scenarios cannot be uniquely ascribed to the pronounced difference in temperature (T= 1023 K vs T= 1173 K) or feed composition (CH_4/O_2= 2 vs CH_4/O_2= 10). To distinguish the two contributions, the impact of operating temperature at constant feed composition was evaluated first (Figure 3/C). Despite the slight increase in the spread of the data, a very strong correlation ($\rho = 0.94$) can be observed between the two data sets, thus suggesting that a 100 K difference in operating temperature only modestly impacts on the catalyst ranking. Consequently, also the top 10% catalysts are not significantly influenced. Similar results were obtained for other pairwise comparisons at fixed feed composition, reported in section S3 of the S.I..

The minor impact of temperature on catalyst ranking is encouraging in terms of comparing isothermal experimental data from different sources. Pronounced deviations from ideal isothermal operation[37, 59], which undoubtedly influence the catalytic performance, might not be the most influential factor in the ranking and, hence, OCM catalyst selection.

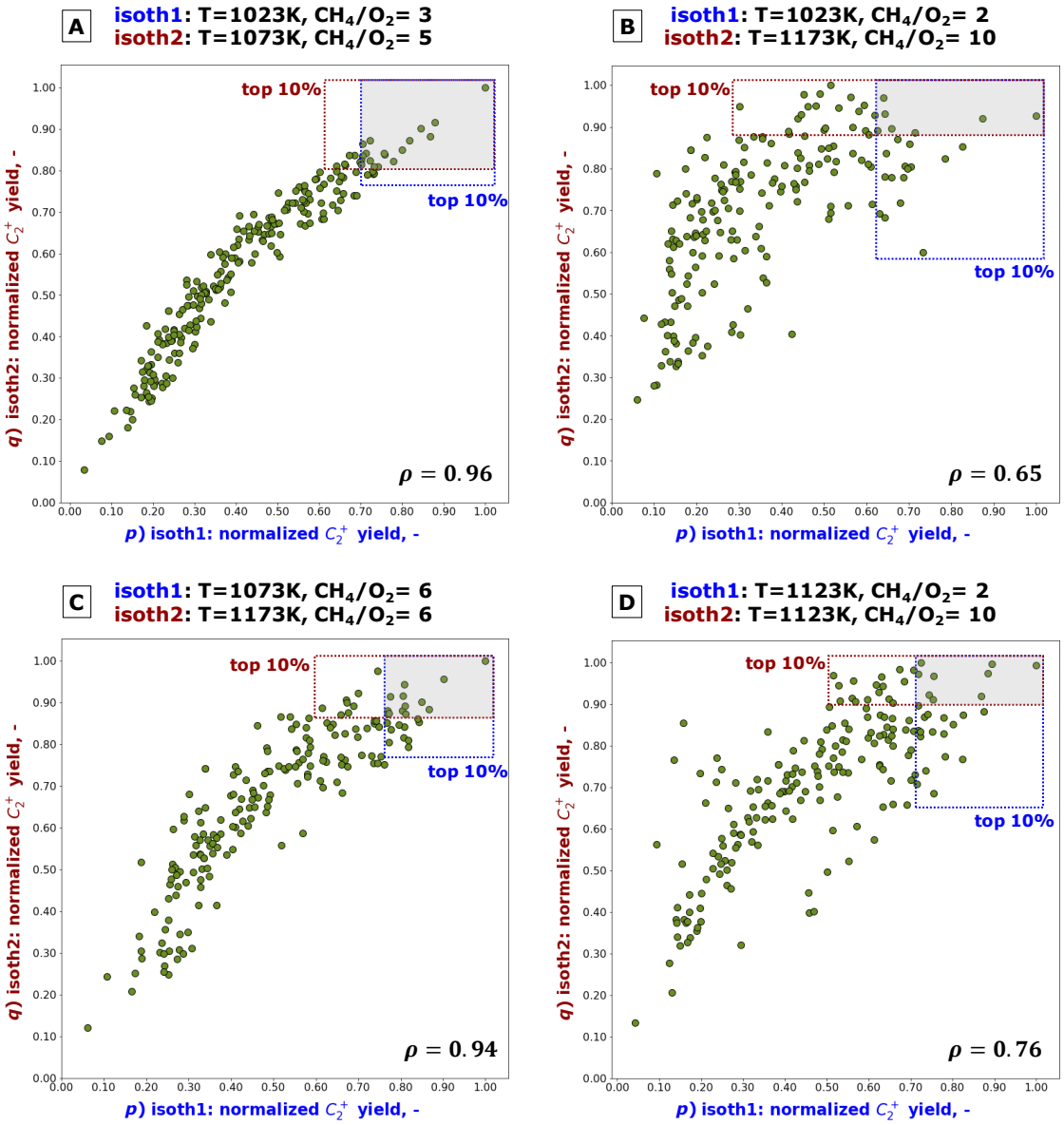

Figure 3. Pairwise comparisons of the performance ranking of the 220 realistic OCM catalysts, for four isothermal scenarios, with operating conditions as indicated in the top legends.

Afterwards, the impact of the methane-to-oxygen ratio at a fixed operating temperature was assessed (Figure 3/D). Although a reasonably strong correlation ($\rho = 0.78$) can still be observed between the two data sets, the spread in the data cannot be ignored and, more

importantly, the top 10% catalysts are largely different in the two scenarios. Similar results were obtained for other pairwise comparisons at fixed operating temperature, reported in section S3 of the S.I..

This result was further investigated by statistically comparing the catalyst descriptors of the top 10% catalysts in both scenarios in Figure 3/D. The statistical results and their detailed kinetic interpretation are reported in section S4 of S.I.. The main conclusion was that the specific concentration of adsorbed atomic oxygen (O*) was significantly lower on the top-performing catalysts in the oxygen-lean scenario, i.e. CH_4/O_2= 10. This surface oxygen species results from the dissociative chemisorption of an oxygen molecule from the gas phase (reaction [1] in Table 2). Such species is responsible for methane activation via hydrogen abstraction (reaction [2] in Table 2) as well as for surface oxidations (e.g. reactions [3] and [4]).

Table 2. Selected elementary steps from the microkinetic model[38], herein reported to facilitate the discussion of the results.

	Elementary step	Description
[1]	$O_{2(g)} + 2* \rightleftharpoons 2O*$	Dissociative oxygen chemisorption
[2]	$CH_{4(g)} + O* \rightleftharpoons CH_{3}\cdot_{(g)} + OH*$	Hydrogen surface abstraction from methane
[3]	$CH_{3}\cdot_{(g)} + O* \rightleftharpoons CH_3O*$	Methyl radical surface oxidation
[4]	$C_2H_{4(g)} + O* \rightleftharpoons C_2H_4O*$	Ethylene surface oxidation
[5]	$CH_{3}\cdot_{(g)} + O_{2(g)} \rightleftharpoons CH_3O\cdot_{(g)} + O\cdot_{(g)}$	Methyl radical gas-phase oxidation
[6]	$CH_{3}\cdot_{(g)} + CH_{3}\cdot_{(g)} \rightleftharpoons C_2H_{6(g)}$	Methyl radicals gas-phase coupling to ethane

A lower concentration of surface oxygen implies lower catalyst activity, but this effect was herein eliminated by comparing catalysts at iso-conversion, rather than iso-space velocity. A high concentration of surface oxygen favours not only methane activation, but also surface oxidation of methyl radicals and ethylene to CO_X. The impact of surface oxygen concentration on selectivity is therefore significant. In fact, a low surface oxygen concentration induces a shift from surface to gas-phase chemistry. This is detrimental in case of an oxygen-rich feed (e.g.

CH_4/O_2= 2) due to non-selective oxidation reactions in the gas phase (e.g. reaction [5] in Table 2), while at oxygen-lean conditions (e.g. CH_4/O_2= 10), the coupling of methyl radicals (reaction [6]) is favoured resulting in a net increase in C_{2+} selectivity at iso-conversion (see Figure S4.3 in S.I.). This qualitative observation, quantified in S.I., is corroborated by Sinev et al.[60], and suggests an optimal concentration of surface oxygen in terms of C_{2+} yield which is directly related to the oxygen concentration in the gas phase.

This hypothesis is in support of the catalyst ranking varying considerably with feed composition. This in turn indicates that performance evaluations of catalysts at low CH_4/O_2 cannot be directly extrapolated to high CH_4/O_2 operation. While this confirms that catalysts should always be designed to the targeted operating conditions[40], it also raises concerns about the applicability of typical bench-scale isothermal tests to catalyst benchmarking to adiabatic operation, due to the difference in methane-to-oxygen ratios for the two cases. These concerns are further elaborated in section 4.1.

Moving to adiabatic operation, the pairwise comparisons for the three adiabatic scenarios are reported in section S5 of S.I. and here only the main conclusion is summarized. The comparisons resulted in very high correlation coefficients (ρ= 0.96 - 0.99), thus testifying that the catalyst ranking was mostly preserved in the considered adiabatic scenarios. As a result, the top 10% OCM catalysts were the same for all three scenarios. It is worth highlighting that, given the imposed constraint on the maximum temperature (1273 K), the investigated range of inlet temperatures (800-900 K) corresponds to a narrow range of oxygen-lean inlet feed compositions (CH_4/O_2= 9-11) and lower methane-to-oxygen ratios could not be considered. The minor differences in catalyst ranking for the three adiabatic scenarios are thus in agreement with the previous results from isothermal scenarios, in which variability in the methane-to-oxygen ratio was pinpointed as the key factor.

3.2 Catalyst ranking in isothermal vs adiabatic operation

The agreement between data from isothermal and adiabatic operation was investigated via four extreme isothermal scenarios, as shown in Figure 4: A) low-temperature and oxygen-rich, B) high-temperature and oxygen-rich, C), low-temperature and oxygen-lean, D) high-temperature and oxygen-lean. In this figure, all four isothermal rankings are compared to the one obtained for an adiabatic scenario at high inlet temperature (T_0= 900 K), for which most catalysts achieve complete oxygen conversion (see also section S.5 in S.I.). The lowest correlation (ρ= 0.51). The is obtained when comparing the adiabatic to the isothermal ranking from scenario A, at low temperature and low methane-to-oxygen ratio. The correlation only marginally improves (ρ= 0.57) when proceeding to scenario B at higher temperature. The effect of an oxygen-lean feed, even at low temperature, is significantly more pronounced (ρ= 0.71). Finally, the best correlation with adiabatic rankings is obtained from isothermal data obtained at high temperature and with an oxygen-lean feed (ρ= 0.86). Similar conclusions can be drawn from evaluating the overlap (C and D) or the lack of overlap (A and B) between the top 10% performing catalysts.

It should be noted that in the case of comparisons such as the ones reported in Figure 4/A and B, the statistical analysis of the top 10% catalysts for the isothermal and adiabatic scenarios did not reveal any significant trend in the descriptors which could explain why so many good performing catalysts in adiabatic operation, i.e., those in the red box, do not exhibit an equally good performance in isothermal operation, i.e., are not within the blue box. Hence, an additional analysis of these extreme cases was carried out.

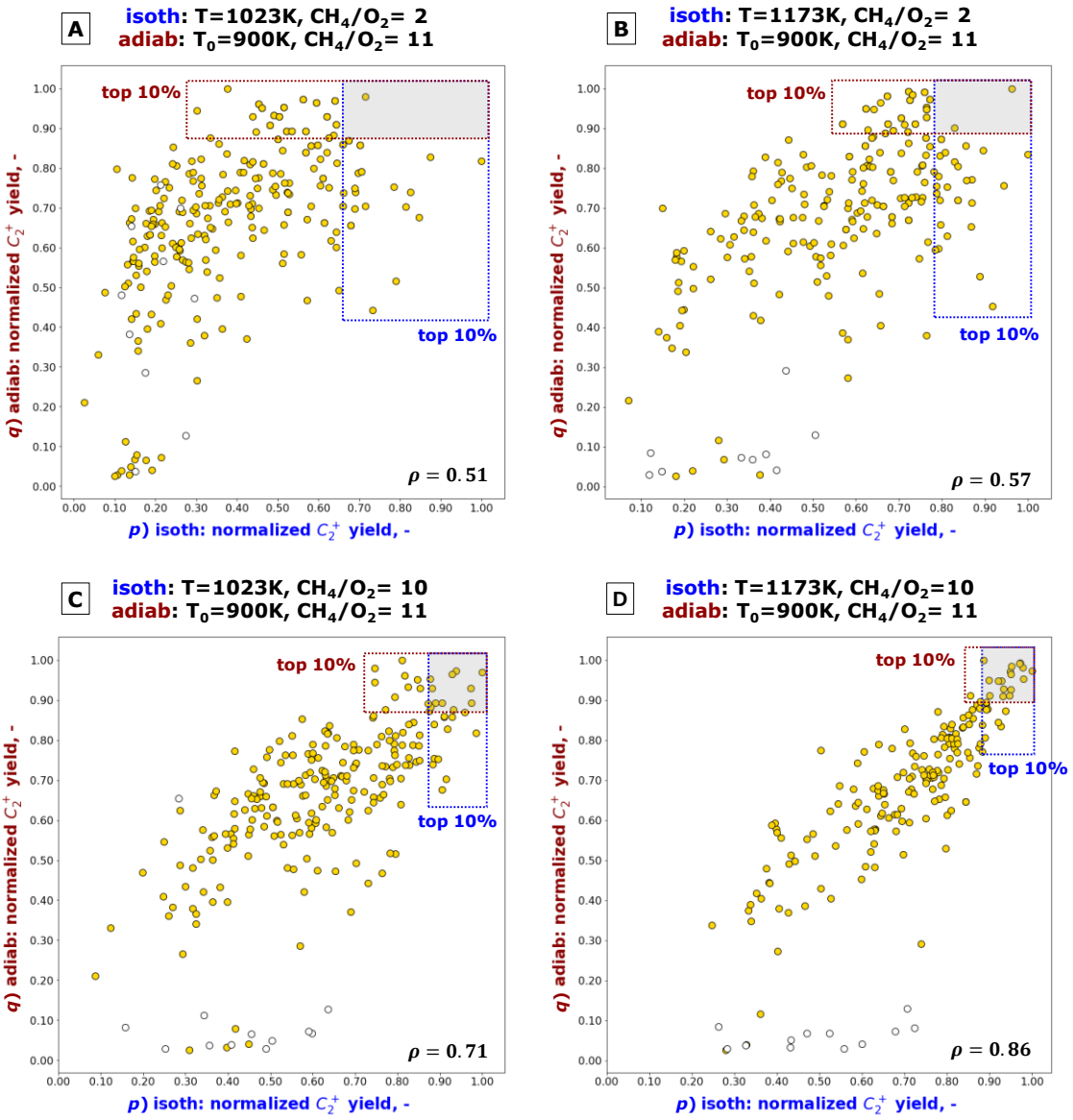

Figure 4. Pairwise comparisons of the performance ranking of the 220 realistic OCM catalysts, for four isothermal scenarios compared to one adiabatic scenario, with operating conditions as indicated in the top legends. Empty circles correspond to catalysts for which oxygen conversion in the adiabatic scenario is below 50% and for this reason are excluded from the analysis of the correlation coefficient.

For the sake of visual clarity, Figure 5 reports the same pairwise comparisons as Figure 4/A and B, but this time indicating the median performances in both scenarios. When focusing on these median performances, rather than on the top 10% oly, one can observe even more clearly that some catalysts, i.e. those in the 1st quadrant of the figures, are ranked poorly in the isothermal scenario but are characterized by above-median ranking in the adiabatic case.

A statistical comparison of the catalyst descriptors of the catalysts belonging to the two highlighted quadrants in Figure 5 revealed that the catalysts in the 1st quadrant oxidize ethylene

more extensively than the catalysts in the 2nd quadrant. As shown in section S7 of the S.I., this difference could be pinpointed to the different values of the sticking probability of ethylene on surface oxygen, which is the catalyst descriptor impacting the pre-exponential factor of reaction [4] in Table 2. The catalyst in the 1st quadrant showed significantly higher sticking probability and, hence, faster ethylene surface oxidation. Hence, most of these 1st quadrant catalysts would have been discarded via a typical isothermal screening, although their adiabatic performance is interesting.

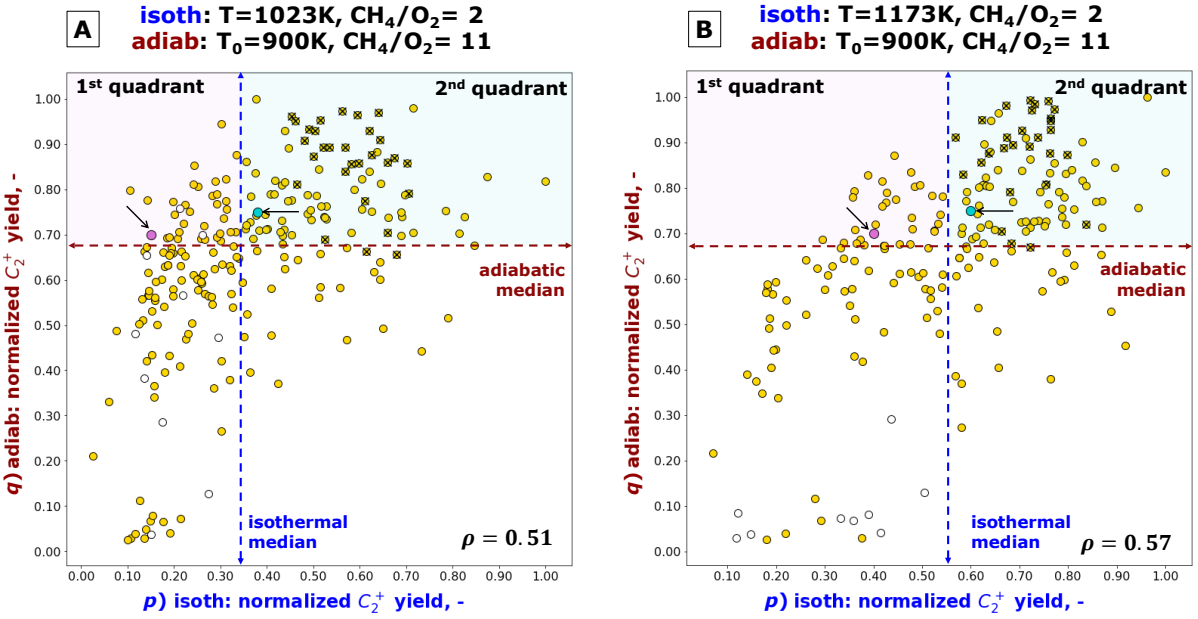

Figure 5. Analogous to Figures 4/A and 4/B. The dashed lines indicate the median rankings for both scenarios considered in each of the two comparisons. The black arrows point to the two catalysts compared in Figure 8. The black crosses are indicative of catalysts which were found to be representative of promoted NaMnW/SiO$_2$ catalysts[46] (see also section S.2 of S.I.).

The catalysts indicated by the black crosses in Figure 5 correspond to combinations of descriptors representative of promoted NaMnW/SiO$_2$ catalysts[52] (see also section S2 in S.I.). It can be observed that almost all these catalysts fall in the 2nd quadrant, being characterized by above-median rankings. This is in agreement with the fact that many of the top-performing catalysts reported in literature belong to this catalyst family[61]. However, promoted NaMnW/SiO$_2$ catalysts have proven to be thermally unstable and, thus, prone to deactivation[55] and alternatives for adiabatic operation shall thus be explored. Therefore, even though not

specifically addressed in the present work, the screening and selection procedure should not disregard issues such as phase transformation, thermal stability and potential deactivation, measured via, for instance, *operando* characterization[61]. If catalysts such as the ones in the 1st quadrant would prove to be more suitable than 2nd quadrant catalysts in this respect, the former would be of higher interest.

Going back to the bigger picture, all pairwise comparisons between the thirty-six isothermal scenarios and the two extreme adiabatic scenarios (T_0= 800 K and T_0= 900 K) are visualized in terms of correlation coefficients in Figure 6 (based on Table S4.1 in S.I.). A high correlation coefficient is indicative of a high predictive power of the isothermal data with respect to the adiabatic scenario considered. The trends reported in this figure show that the adiabatic catalyst ranking is more adequately predicted by the catalyst ranking derived from isothermal data obtained at high temperature (≥ 1123 K) and high CH_4/O_2 (≥ 7). These results are in agreement with what was observed in section 3.1 for isothermal scenarios only and confirm that the evaluation of adiabatic catalytic performances based only on conventional isothermal experimentation can lead to the selection of a suboptimal catalyst.

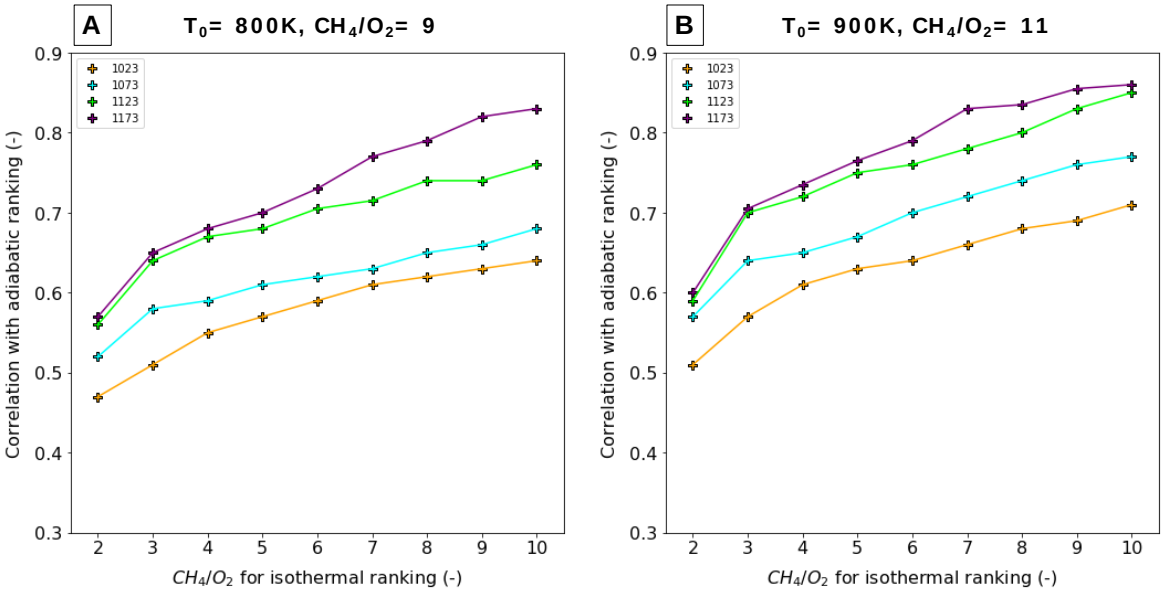

Figure 6. Overview of the correlation coefficients between adiabatic and isothermal rankings as a function of the isothermal methane-to-oxygen ratios at four different isothermal operating temperatures, for two adiabatic scenarios (A and B).

4. Discussion

4.1 Surveying isothermal data from an adiabatic perspective

As the performance of OCM catalysts in adiabatic operation is not always well represented by bench-scale data acquired at typical isothermal conditions, it is judicious to revise isothermal data from literature. A minimum limit for an economically-profitable industrial implementation (C_2 yield≥ 15%[62]) was used as a criterion to select 387 experimental data points from the database reported by Schmack et al.[14] (shown in Figure 7/A). The average temperature and methane-to-oxygen molar feed ratio amount to 1041 K and 3 respectively, in line with the typical operating range of isothermal conditions considered in the present work (CH_4/O_2= 2-5, T= 1023-1073 K). Actually the typical range leads to an average C_2 yield of approx. 33% higher than the average yield obtained in the interval CH_4/O_2= 5-10, T= 1073-1173 K (10.6% for the former vs 8.0% for the latter). This difference can be attributed to higher methane conversion (22.5% vs 13.4%) when operating closer to the stoichiometric feed composition (CH_4/O_2= 2-5), despite the reduction in the average C_2 selectivity (from 59.4% to 47.1%). However, such typical range is far from the most relevant isothermal conditions for catalyst selection in adiabatic operation (T≥ 1123K and CH_4/O_2≥ 7), identified in section 3.2.

Figure 7/B displays a data subset acquired at these relevant high temperatures and high CH_4/O_2 ratios. Comparison with Figure 1 shows that only approximately 5% of all catalytic tests considered have been performed within this range of interest. The reason why these conditions are not often screened can be attributed to low C_2 yields (6.7% on average) resulting from the limited methane conversion at high methane-to-oxygen feed ratios. The subset in Figure 7/B suggests that none of the most widely studied OCM catalysts, such as promoted Li/MgO[63] and NaMnW/SiO_2[64], have been tested (and/or showed any remarkable performance) at conditions relevant for adiabatic operation.

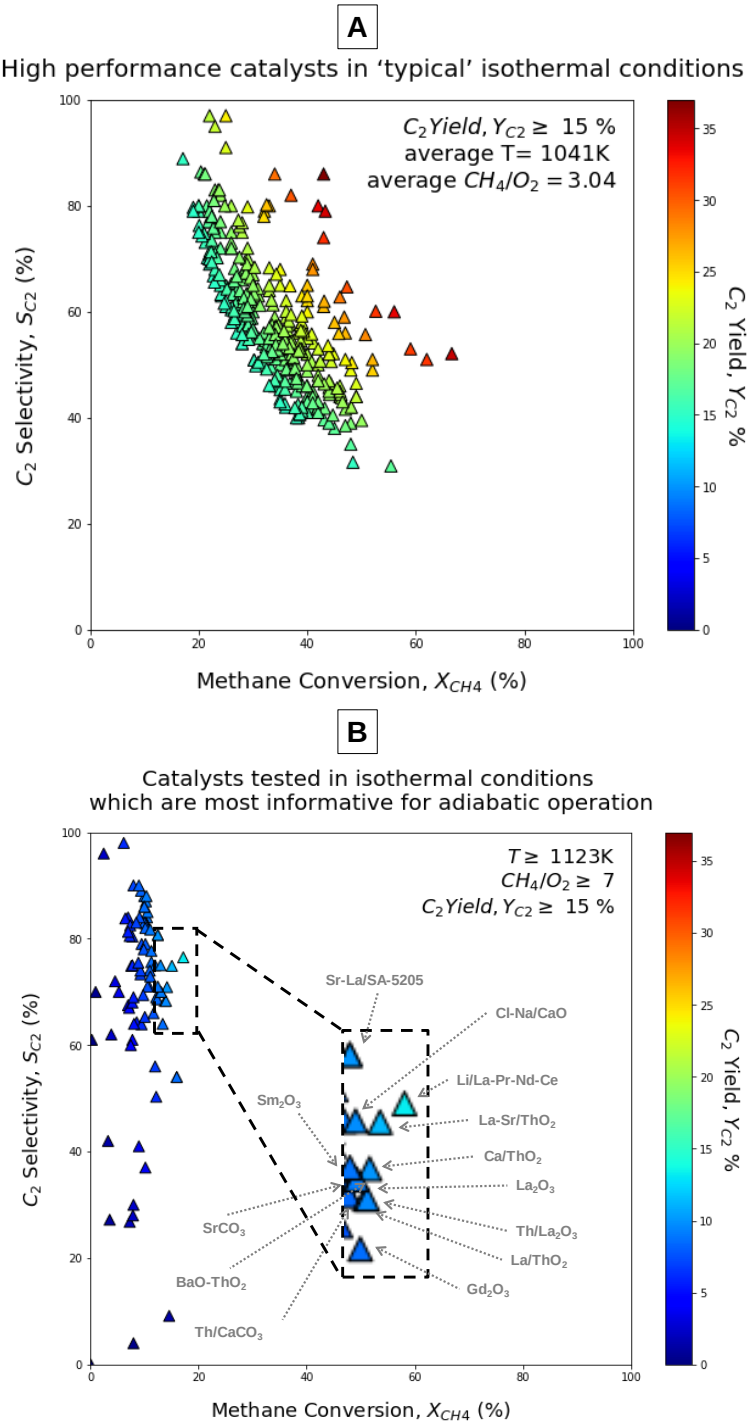

Figure 7. Selection of isothermal experimental data available in literature for OCM catalysts [14] A) 387 datapoints commonly considered of interest for isothermal OCM, thanks to the high (≥15%) yield. B) 81 datapoints obtained at operating conditions leading to high correlation with adiabatic data, namely high temperature (≥ 1123 K) and more importantly high CH_4/O_2 (≥ 7).

In conclusion, 95% of the OCM catalysts tested already were done at conditions in which their performance was not sufficiently informative for their application in an adiabatic reactor. Thus, prior to the synthesis of new, ad-hoc materials for adiabatic OCM, testing of already available

materials in conventional isothermal operation, but focusing on high CH_4/O_2 and high temperature operation, is recommended as first step in the search for promising catalysts in adiabatic operation.

4.2 Mechanistic insights into suitable catalysts for adiabatic operation

The analysis of literature data as performed in section 4.1, together with the lack of predictive power of typical isothermal data, suggests that high-performing catalysts according to conventional isothermal screening should not necessarily be the focus of adiabatic-oriented OCM research. To gain further fundamental understanding into these discrepancies in the catalyst ranking between the two operating modes, an additional kinetic investigation was performed. To do so, the focus was put on two catalysts representative of the two quadrants previously identified in Figure 5. These catalysts were carefully selected, such that the only dissimilar catalyst descriptor between the two would be the sticking probability of ethylene on a surface oxygen (high value , $1.1 \cdot 10^{-4}$, for the 1st quadrant catalyst and low value, $2.7 \cdot 10^{-5}$, for the 2nd quadrant catalyst).

In Figure 8, the first-rank Delplot[65], i.e. the C_{2+} selectivity as a function of O_2 conversion, is reported in several scenarios for the two catalysts. It can be observed that, since no ethylene is present at the inlet of the reactor, the two catalysts exhibit comparable selectivity in the low conversion range. This selectivity is below 100%, which is typical for most OCM catalysts, meaning that a portion of the $CH_3\cdot$ radicals generated by methane activation on the catalyst surface is immediately oxidized to carbon (di)oxide, either in the gas phase or on the catalyst surface (primary oxidation). However, the differences in C_2H_4 surface oxidation (consecutive oxidation), arising from the different sticking coefficient considered for the two catalysts, are translated into a much steeper decrease in selectivity with conversion for the 1st quadrant catalyst in both the isothermal scenarios (Figure 8/A and B). This effect is particularly striking

in Figure 8/A, corresponding to an isothermal scenario with a low temperature and low CH_4/O_2, i.e. the most typical, but not the most adiabatically-relevant.

Although still present, the differences in the evolution of selectivity with O_2 conversion are less pronounced in high-temperature and high methane-to-oxygen ratio isothermal operation (Figure 8/B) and even less pronounced in adiabatic operation (Figure 8/C and D). Such observation points to consecutive oxidation being less relevant under such conditions, explaining hence the comparable adiabatic rankings for the catalysts in the two quadrants, despite the significant differences in the isothermal rankings.

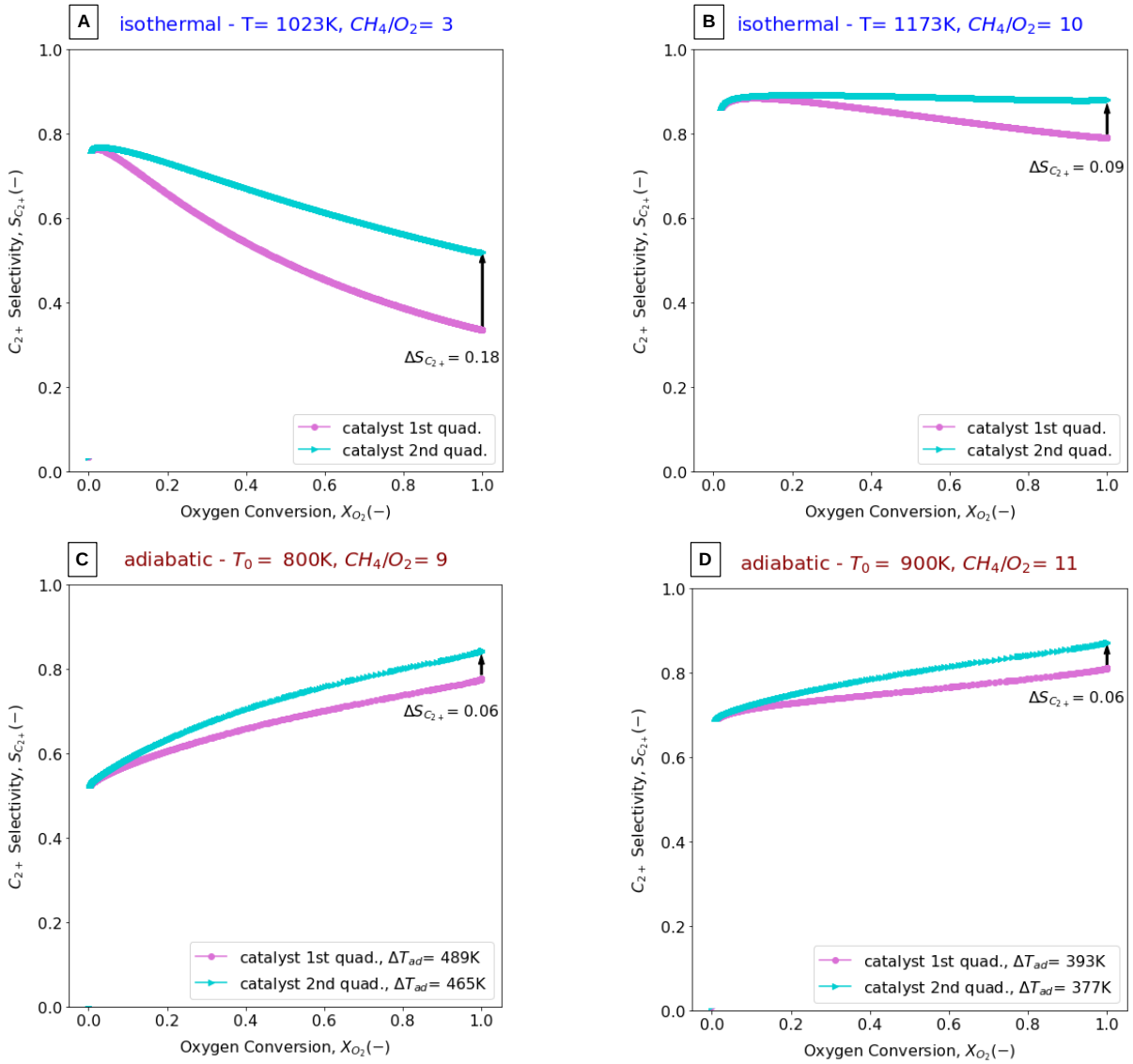

Figure 8. First-rank Delplots, i.e. selectivity vs conversion plots, for two catalysts belonging to the 1st (pink) and 2nd (light-blue) quadrants of Figure 5, for two isothermal (A, B) and two adiabatic scenarios (C,D), with operating conditions as indicated in the top legends.

In order to have a complete view on the impact of operating temperature and methane-to-oxygen ratio on the prevailing oxidation routes, additional results and discussion on the isothermal scenarios are reported in section S7 of the S.I.. Only the main conclusions on are herein reported.

As expected, temperature was found to have an effect on the absolute performances of the two catalysts, reducing the importance of both primary and consecutive oxidation[66]. This beneficial effect of higher temperature on the reaction kinetics is also the cause for the increase in selectivity with conversion observed for the two adiabatic cases (Figure 8/C and D), with higher conversion resulting in higher temperatures, as indicated by the adiabatic temperature rise reported in the figure. However, temperature alone was found not to be the primary driver in the change in catalyst ranking between the isothermal and adiabatic scenarios, with the effect CH_4/O_2 being again more pronounced. In fact, the consecutive oxidation of the products was found to be much less significant in an oxygen-lean environment (high CH_4/O_2) thanks to the reduced availability of the oxidant. Mainly, because the limited amount of oxygen in the gas phase is already consumed in the unavoidable and undesired oxidation of $CH_3\cdot$ radicals[37].

This conclusion is in agreement with the previous observations and reasoning behind a lower surface concentration of O* active species being preferred in oxygen-lean conditions. Additionally, catalyst selection for adiabatic operation based on isothermal screening would thus benefit from a preliminary assessment of the extent of C_2 oxidation on the catalyst surface. Hence, it is advisable to compare catalytic performances as a function of conversion, rather than relying on comparisons at a single fixed conversion, in order to follow the selectivity evolution. As shown above, this approach can provide a simple and effective comparison of the prevailing oxidation routes (primary and consecutive) for different catalysts, hence facilitating the extrapolation of isothermal evaluations to the adiabatic case.

5. Conclusions

The challenge of extrapolating the decades-long extensive isothermal experimentation on OCM catalysts to the recent shift of industrial interest towards adiabatic operation was addressed via microkinetic simulations. Surprisingly, for both isothermal and adiabatic operating modes the operating temperature was found not to be the most decisive factor in catalyst ranking in terms of C_{2+} yield. Rather, the methane-to-oxygen feed ratio affects this catalyst ranking more significantly. As a matter of fact, in case of high gas-phase oxygen concentration (CH_4/O_2= 2), catalysts with a higher concentration of surface oxygen species were found to perform better, while the opposite was true in case the gas phase was oxygen-lean (CH_4/O_2= 10). At oxygen-rich conditions, a high surface oxygen concentration is needed to reduce the impact of gas-phase reactions (and oxidation in there), while at oxygen-lean conditions a lower surface oxygen concentration is preferred because then the undesired oxidation would mainly occur on the surface. Isothermal data obtained at low CH_4/O_2 are typically associated with high C_{2+} yields and have been generally considered of higher interest. However, for the reasons above, these data could lead to misleading conclusions in catalyst selection for adiabatic operation, in which high oxygen contents are avoided to keep the adiabatic temperature rise under control.

These insights can be translated into practical guidelines for the planning of new bench-scale isothermal experiments aimed at catalyst screening for adiabatic operation. For catalyst ranking, it is indeed advisable to evaluate performances in an oxygen-lean environment (i.e. $CH_4/O_2 \geq$ 7) and, preferably, at high temperature (i.e. $\geq$ 1123 K). Additionally, experiments at variable space-time enable the comparison of the selectivity evolution with conversion, to gain preliminary mechanistic understanding about the surface oxidation pathways, which was found to significantly impact the different ranking of the catalyst candidates. In view of these simple guidelines, it is proposed to re-evaluate at more relevant conditions not only the top-performing catalysts identified so far but also known catalyst formulations that have been discarded

previously, especially if the low yields were suspected to be due mainly to selectivity loss in consecutive surface oxidation.

Supplementary Information

S1. Overview of the OCM microkinetic and reactor model; S2. Catalysts and realistic sets of catalyst descriptors; S3. Additional results about catalyst ranking in isothermal operation; S4. Additional results about the feed composition effect in isothermal operation; S5. Results about catalyst ranking in adiabatic operation; S5.Additional results about catalyst ranking in isothermal vs adiabatic operation; S7. Additional results about the comparison of 1st quadrant and 2nd quadrant catalysts.

Nomenclature

CH_4/O_2	methane-to-oxygen molar ratio at the inlet of the reactor
ΔT_{ad}	adiabatic temperature rise (K)
F	molar flowrate at the outlet of the reactor (mol/s)
F_0	molar flowrate at the inlet of the reactor (mol/s)
GHSV	gas hourly space velocity $\left(\frac{m^3_{gas}\vert_{STP}/h}{m^3_{catalyst}} = h^{-1}\right)$
n	number of realistic OCM catalysts
p	first operating scenario in each pairwise comparison (x-axis in the figures)
q	second operating scenario in each pairwise comparison (y-axis in the figures)
$\dot{Q}$	cooling capacity (W)
$\dot{Q}_R$	generated power (W)
ρ	Pearson's correlation coefficient
S_{C_2}	selectivity towards C_2 products (C_2H_6, C_2H_4, C_2H_2); $S_{C_2} = \frac{2\times(F_{C2} - F_{C2,0})}{F_{CH4,0} - F_{CH4}}$

S.I.	supplementary information
T	operating temperature in an isothermal reactor (K)
T_0	inlet temperature in an adiabatic reactor (K)
X_{O_2}	oxygen conversion at the reactor outlet; $X_{O_2} = \frac{F_{O2,0} - F_{O2}}{F_{O2,0}}$
X_{CH_4}	methane conversion at the reactor outlet; $X_{CH_4} = \frac{F_{CH4,0} - F_{CH4}}{F_{CH4,0}}$
$Y_{C_{2+}}$	yield of C_{2+} products (C_2H_6, C_2H_4, C_2H_2, C_3H_8, C_3H_6); $Y_{C_2+} = X_{CH_4} \times S_{C_{2+}}$

Conflicts of interest

There are no conflicts of interest to declare.

Acknowledgments

This work was supported by a research program agreement between TOTAL Research & Technology Feluy and Ghent University. The main results from this work were presented during the 12th Natural Gas Conversion Symposium (02-06/06/19, San Antonio – TX). The computational resources (Stevin Supercomputer Infrastructure) and services used in this work were provided by the VSC (Flemish Supercomputer Center), funded by Ghent University, FWO and the Flemish Government – department EWI. JWT acknowledges the ERC for the PoC grant SERENiTi (GA 825783).

References

1. A. Al-Douri, D. Sengupta and M. M. El-Halwagi, *J. Nat. Gas Sci. Eng.*, 2017, **45**, 436-455.
2. IEA, *Outlook for natural gas*, World Energy Outlook 2018, 2018.
3. P. Schwach, X. L. Pan and X. H. Bao, *Chem. Rev.*, 2017, **117**, 8497-8520.
4. B. L. Farrell, V. O. Igenegbai and S. Linic, *ACS Catal.*, 2016, **6**, 4340-4346.

5. Y. Gao, L. M. Neal, D. Ding, W. Wu, C. Baroi, A. Gaffney and F. Li, *ACS Catal.*, 2019, **9**, 8592-8621.
6. J. H. Lunsford, *Catal. Today*, 1990, **6**, 235-259.
7. J. A. Labinger, *Catal. Lett.*, 1988, **1**, 371-375.
8. V. I. Lomonosov and M. Y. Sinev, *Kinetics and Catalysis*, 2016, **57**, 647-676.
9. M. Ravi, V. L. Sushkevich, A. J. Knorpp, M. A. Newton, D. Palagin, A. B. Pinar, M. Ranocchiari and J. A. van Bokhoven, *Nature Catalysis*, 2019, **2**, 485-494.
10. Y. Gambo, A. A. Jalil, S. Triwahyono and A. A. Abdulrasheed, *J. Ind. Eng. Chem.*, 2018, **59**, 218-229.
11. A. Cruellas, T. Melchiori, F. Gallucci and M. van Sint Annaland, *Catal. Rev. Sci. Eng.*, 2017, **59**, 234-294.
12. S. Pak and J. H. Lunsford, *Appl. Catal. A-Gen.*, 1998, **168**, 131-137.
13. K. Van der Borght, K. Toch, V. V. Galvita, J. W. Thybaut and G. B. Marin, *Catalysts*, 2015, **5**, 1948-1968.
14. R. Schmack, A. Friedrich, E. V. Kondratenko, J. Polte, A. Werwatz and R. Kraehnert, *Nature Communications*, 2019, **10**, 441.
15. A. Cruellas, J. J. Bakker, M. van Sint Annaland, J. A. Medrano and F. Gallucci, *Energy Conv. Manag.*, 2019, **198**, 111789.
16. A. A. Latimer, A. Kakekhani, A. R. Kulkarni and J. K. Nørskov, *ACS Catal.*, 2018, **8**, 6894-6907.
17. W. P. Schammel, J. Wolfenbarger, M. Ajinkya, J. McCarty, J. M. Cizeron, S. Weinberger, J. D. Edwards, D. Sheridan, E. C. Scher and J. Mccormick, US Patent, *20140107385A1*, 2014.
18. A. H. Tullo, https://cen.acs.org/business/petrochemicals/McDermott-buys-Siluria-oxidative-methane/97/i32, (accessed 20/08/2019).

19. https://www.linde-engineering.com/en/process_plants/petrochemical-plants/oxidative-coupling-methane/index.html, (accessed 08/10/2018).
20. A. Cruellas, T. Melchiori, F. Gallucci and M. van Sint Annaland, *Energy Technology*, 2019, 1900148.
21. D. W. Leyshon and R. A. Bader, US Patent, *4,876,409*, 1989.
22. D. W. Leyshon, *Stud. Surf. Sci. Catal.*, 1991, **61**, 497-507.
23. C. T. Tye, A. R. Mohamed and S. Bhatia, *Chem. Eng. J.*, 2002, **87**, 49-59.
24. A. Aseem, G. G. Jeba, M. T. Conato, J. D. Rimer and M. P. Harold, *Chem. Eng. J.*, 2018, **331**, 132-143.
25. S. Sarsani, D. West, W. G. Liang and V. Balakotaiah, *Chem. Eng. J.*, 2017, **328**, 484-496.
26. S. Sarsani, D. West, V. Balakotaiah, W. Liang and J.Banke, Patent, WO2018146591Al, 2018.
27. Z. Sun, A. Kota, S. Sarsani, D. H. West and V. Balakotaiah, *Chem. Eng. J.*, 2018, **343**, 770-788.
28. L. Pirro, A. Obradović, B. D. Vandegehuchte, G. B. Marin and J. W. Thybaut, *Ind. Eng. Chem. Res.*, 2018, **57**, 16295-16307.
29. W. Liang, D. West, L. Li, V.S.R. Sarsani, H. Perez, J.W. Kauffman, Patent, *WO2018175535A1*, 2018.
30. W. Liang, V.S.R. Sarsani, D. West, I. Lengyel, Patent, *WO2018048629A1*, 2018.
31. X. Wu, Z. Du, E. Xu and Q. Tang , Patent, *CN106831306A*, 2017.
32. L. A. Vandewalle, I. Lengyel, D. H. West, K. M. Van Geem and G. B. Marin, *Chem. Eng. Sci.*, 2019, **199**, 635-651.
33. V. Balakotaiah, Z. Sun and D. H. West, *Chem. Eng. J.*, 2019, **15**, 1403-1419.
34. P. Stoltze, *Progr. Surf. Sci.*, 2000, **65**, 65-150.

35. H. Gossler, L. Maier, S. Angeli, S. Tischer and O. Deutschmann, *Catalysts*, 2019, **9**, 227.
36. B. Zohour, D. Noon and S. Senkan, *ChemCatChem*, 2014, **6**, 2815-2820.
37. Z. Liu, J. P. Ho Li, E. Vovk, Y. Zhu, S. Li, S. Wang, A. P. van Bavel and Y. Yang, *ACS Catal.*, 2018, **8**, 11761-11772.
38. P. N. Kechagiopoulos, J. W. Thybaut and G. B. Marin, *Ind. Eng. Chem. Res.*, 2014, **53**, 1825-1840.
39. V. I. Alexiadis, M. Chaar, A. C. van Veen, M. Muhler, J. W. Thybaut and G. B. Marin, *Appl. Catal. B-Environ.*, 2016, **199**, 252-259.
40. J. W. Thybaut, J. J. Sun, L. Olivier, A. C. Van Veen, C. Mirodatos and G. B. Marin, *Catal. Today*, 2011, **159**, 29-36.
41. J. Sun, J. W. Thybaut and G. B. Marin, *Catal. Today*, 2008, **137**, 90-102.
42. S. Lim, J.W. Choi, D. J. Suh, K. H. Song, H. C. Ham and J.M. Ha, *J. Catal.*, 2019, **375**, 478-492.
43. K. Takahashi, I. Miyazato, S. Nishimura and J. Ohyama, *ChemCatChem*, 2018, **10**, 3133-3133.
44. E. Y. Chung, W. K. Wang, S. G. Nadgouda, D. S. Baser, J. A. Sofranko and L.S. Fan, *Ind. Eng. Chem. Res.*, 2016, **55**, 12750-12764.
45. P. Schober, C. Boer and L. A. Schwarte, *Anesthesia & Analgesia*, 2018, **126**, 1763–1768.
46. B. Ratner, *J. Target. Meas. Anal. Market.*, 2009, **17**, 139-142.
47. S. Zacks, in *Parametric Statistical Inference*, ed. S. Zacks, Pergamon, 1981, 1-14.
48. W. H. Kruskal and W. A. Wallis, *J. Am. Stat. Assoc.*, 1952, **47**, 583-621.
49. L. Pirro, P. S. F. Mendes, S. Paret, B. D. Vandegehuchte, G. B. Marin and J. W. Thybaut, *Catal. Sci. Technol.*, 2019, **9**, 3109-3125.

50. E. V. Kondratenko, M. Schluter, M. Baerns, D. Linke and M. Holena, *Catal. Sci. Technol.*, 2015, **5**, 1668-1677.
51. L. Olivier, S. Haag, H. Pennemann, C. Hofmann, C. Mirodatos and A. C. van Veen, *Catal. Today*, 2008, **137**, 80-89.
52. K. Huang, X. L. Zhan, F. Q. Chen and D. W. Lu, *Chem. Eng. Sci.*, 2003, **58**, 81-87.
53. S. M. K. Shahri and A. N. Pour, *J. Nat. Gas Chem.*, 2010, **19**, 47-53.
54. P. Crook, *Adv. Mater. Process.*, 2007, **165**, 31-33.
55. N. S. Hayek, G. J. Khlief, F. Horani and O. M. Gazit, *J. Catal.*, 2019, **376**, 25-31.
56. M. Albrecht, U. Rodemerck, D. Linke and E. V. Kondratenko, *React. Chem. Eng.*, 2018, **3**, 151-154.
57. S. Stunkel, H. Trivedi, H. R. Godini, S. Jaso, N. Holst, S. Arndt, J. Steinbach and R. Schomacker, *Chem. Ing. Tech.*, 2012, **84**, 1989-1996.
58. S. Duggal, G. Radaelli, J. Mccormick, A. Aronson, J. Cizeron, D. Jonnavittula, US Patent, *20170107162A1*, 2017.
59. B. Zohour, D. Noon and S. Senkan, *ChemCatChem*, 2013, **5**, 2809-2812.
60. M. Y. Sinev, Z. T. Fattakhova, V. I. Lomonosov and Y. A. Gordienko, *J. Nat. Gas Chem.*, 2009, **18**, 273-287.
61. D. Kiani, S. Sourav, J. Baltrusaitis and I. E. Wachs, *ACS Catal.*, 2019, **9**, 5912-5928.
62. E. V. Kondratenko, T. Peppel, D. Seeburg, V. A. Kondratenko, N. Kalevaru, A. Martin and S. Wohlrab, *Catal. Sci. Technol.*, 2017, **7**, 366-381.
63. S. Arndt, G. Laugel, S. Levchenko, R. Horn, M. Baerns, M. Scheffler, R. Schlogl and R. Schomacker, *Catal. Rev.Sci. Eng.*, 2011, **53**, 424-514.
64. S. Arndt, T. Otremba, U. Simon, M. Yildiz, H. Schubert and R. Schomäcker, *Appl. Catal. A – Gen.*, 2012, **425-426**, 53-61.
65. N. A. Bhore, M. T. Klein and K. B. Bischoff, *Ind. Eng. Chem. Res.*, 1990, **29**, 313-316.

636 66. M. Y. Sinev, Z. T. Fattakhova, V. I. Lomonosov and Y. A. Gordienko, *J. Nat. Gas*
637 *Chem.*, 2009, **18**, 273-287.